JGISE Vol. 7 No. 2 (2024), pp. 171 - 182 | https://doi.org/10.22146/jgise.102075

JGISE
Journal of Geospatial Information Science and Engineering
ISSN: 2623-1182 | https://jurnal.ugm.ac.id/jgise

Bathymetric Mapping of Shallow Water Using Aerial Images with Structure-From-Motion Approach: A Case Study of Kepulauan Seribu Water, Jakarta

(*Bathymetric Mapping of Shallow Water Using Aerial Images with Structure-From-Motion Approach: A Case Study of Kepulauan Seribu Water, Jakarta Pemetaan Batimetri Perairan Dangkal Menggunakan Citra Udara dengan Pendekatan Structure-From-Motion: Studi Kasus Perairan Kepulauan Seribu, Jakarta*)

Teguh Sulistian, Herjuno Gularso, Dewi Sekar Arum, Sandi Aditya, Fajar Triady Mugiarto

The Geospatial Information Agency, Indonesia

Penulis Korespondensi: Teguh Sulistian **| Email:** teguh.sulistian@big.go.id

Diterima (*Received*): 02/Dec/2024 Direvisi (*Revised*): 27/Dec/2024 Diterima untuk Publikasi (*Accepted*): 27/Dec/2024

ABSTRACT

Bathymetric mapping is crucial for marine spatial planning and coastal infrastructure development. However, shallow waters ranging from 0 to 5 meters are considered critical areas that pose dangers to conventional survey vessels. This research examines a bathymetric mapping method for the shallow waters of Kepulauan Seribu, Jakarta, using aerial images captured by an unmanned aerial vehicle (UAV) with a structure-from-motion (SfM) approach. Furthermore, the point cloud must be corrected for the refractive index since light passes through air and water. The seawater refractive index is derived from salinity and seawater temperature data. The validation process uses several independent control points (ICPs) obtained from GNSS real-time kinematic (RTK) measurements and soundings conducted with an unmanned surface vessel (USV). The accuracy assessment shows that the SfM point cloud data has a horizontal RMSE of 0.103 m and a vertical RMSE of 0.191 m. The aerial image approach significantly speeds up the acquisition process compared to conventional sounding methods. It produces a higher density of point clouds, integrating the coastal digital elevation model (DEM) of both land and sea areas. However, the use of this method is limited to clear waters where the seabed is visible in the images.

Keywords: bathymetry mapping, shallow water, aerial photogrammetry, SfM, base map, coastline

1. Introduction

Indonesia is a maritime country with tremendous potential for marine resources. Beyond fisheries, the marine economic potential can be developed through various sectors, such as aquaculture, fish processing, port services, exploration of offshore energy resources, coastal forestry, trade, shipping, and tourism (Hanim & Noorman, 2016). To manage and optimize these benefits, marine spatial planning plays a critical role in achieving sustainability. Spatial planning significantly impacts several aspects of sustainability (Terama et al., 2019). One of the most essential datasets for marine spatial planning is depth information, which can be represented in a marine base map.

Various methods can achieve high accuracy in depth information or bathymetric data, such as single beam echosounder (SBES) sounding. However, shallow waters with 0–5 meters present a challenge, as these critical areas are dangerous for conventional survey vessels to navigate. Instead of using conventional vessels, Unmanned Surface Vehicles (USVs) offer significant advantages with their advanced capabilities in communication, observation, perception, safety, and navigation reliability (Bai et al., 2022). USVs can be used as an alternative to conduct SBES sounding in shallow waters. On land, the Real-Time

Kinematic (RTK) method can be employed for topographic data acquisition. Nonetheless, this method faces challenges related to its measurement capacity and land cover characteristics, such as mangroves and cliffs in coastal areas. Moreover, RTK surveys typically require more time to complete (Nugraha, 2018).

According to Gularso et al. (2021), generating a digital elevation model (DEM) from aerial images using an image-matching approach is possible and can address the limitations of conventional geospatial data acquisition methods. Aerial images can be captured using non-metric cameras mounted on Unmanned Aerial Vehicles (UAVs). However, their research was limited to DEM extraction on land areas only and did not include sea areas. In addition, red LiDAR laser method cannot penetrate water because water is a strong absorber, which the higher wavelength of typical LiDAR sensors prevents them from penetrating water (Awadallah,2021).

Other studies have demonstrated that bathymetric data can be obtained from aerial images captured by UAVs equipped with non-metric cameras, using advanced photogrammetry approaches such as Structure from Motion (SfM). The high-resolution bathymetric models developed from SfM method can provide finer-scale and more robust measurements of seafloor bathymetry (Storlazzi, 2016). This method provides efficient, flexible, fast, and cost-effective data acquisition and can be optimized to fill gaps in geospatial data in coastal areas. The SfM method is effective in certain conditions, such as clear water environments, calm waves, and visible seabed conditions. However, it is less suitable for areas with turbid water, large waves, or homogeneous sandy seabeds (Slocum et al., 2019).

Applying the SfM method for bathymetry data extraction requires consideration of several factors, including wave dynamics and light refraction. In coastal areas with significant wave activity, depth correction is necessary by calculating the inverse of wave speed at each wave crest. Additionally, predicting long-wave patterns and eliminating short-wave effects can enhance bathymetric data accuracy (Matsuba & Sato, 2018). Furthermore, aerial image acquisition should be conducted during calm wave conditions to minimize error. Another factor influencing the accuracy of the resulting DEM is light refraction when the photo light enters the water. Due to differences in refractive indices between air and water, the measured depth often appears shallower than the actual depth (Dietrich, 2017). Additionally, the iterative Dietrich's refraction-correction method improved the accuracy of generating shallow stream bathymetry from multi-view stereo photogrammetry (MVS-SfM) and utilization of raster data files is more efficient compared to point cloud processing (Lingua et al.,2023). However, this research will examine point cloud processing workflow.

This research focuses on extracting bathymetric data from aerial images captured by non-metric cameras using the SfM approach. The study also aims to assess the accuracy and efficiency of the data acquisition process.

2. Material and Methods

2.1. Data and Location

Field data was collected between 27 August and 2 September 2021 in the Kepulauan Seribu Administrative District, DKI Jakarta, covering eight islands: Kelapa Dua, Kelapa, Harapan, Panggang, Pramuka, Tidung Besar, Tidung Kecil, and Payung Islands. These islands are part of the Kepulauan Seribu National Park, a protected area within the province of Jakarta. The location of the research area can be seen in Figure 1.

Figure 1 Research area

2.2. Methodology

The equipment used in this study included UAVs for aerial image acquisition, GNSS receivers for ground control points, and USVs for sounding. Detailed specifications are presented in Table 1.

The methodology in this research is illustrated in the flow chart of Figure 2. The research process comprises four main stages: preparation, data collection, processing, and accuracy analysis (refer to Figure 2). This section describes how the research is conducted, including the research design, data collection techniques, instrument development, and data analysis methods.

Table 1 Equipment specification

Equipment	Specifications
UAV: Matrice 600	a. Diagonal wheelbase: 895 mm b. Maximum Speed: 17 m/s c. Maximum flight time: 40 min
Camera: Alpha Air 450	a. Resolution: 6000x4000 b. Effective pixel: 24,3 MP
Receiver GNSS Trimble R8S	a. Positioning Rates: 1 Hz, 2Hz, 5Hz, 10 Hz dan 20Hz b. RTK method precision Horizontal 8mm+1 ppm RMS, vertical 15mm+ 1 ppm RMS
USV Hi-Target I-Boat BS3	a. Dimension 1100mm x 520mm x 300mm b. Range Telemetry 1,5 km c. Positioning DGNSS Veripos LD8 Ultra Correction d. Frequency SBES 200 khz e. Sounding Accuracy 1 cm ± 0.1%h (h=depth), 1cm sounding resolution
Valeport SVP Midas	a. Temperature range: -5°C to +35°C, accuracy: ±0.01°C b. temperature range: 10, 50, 100, 300 or 600bar, accuracy ±0.01% range
Laptop Workstation: Dell Precision 7550	a. Intel Xeon W-10885M CPU @ 2,4GHz (16 CPU) b. Memory: 64GB RAM
Aerial Image Processing Software: Agisoft	a. Can process aerial image using Structure from Motion method b. Can generate dense point cloud
Refractive Correction Processing Software	a. Can calculate refractive index in water area b. Can calculate refractive correction of SfM resulted point cloud c. MATLAB-language software developed by authors himself
DEM extraction Software: Generic Mapping Tools (GMT)	open-source software for gridding and extract DEM from corrected point cloud data

2.3. Flight Plan

The flight plan covered seven islands and was conducted using a UAV. The plan was designed to capture the entire mainland area up to the edges, ensuring that all corals and shallow water areas were included in the acquisition zone (see Figure 3). The acquisition plan was designed with 90% overlap and 70% sidelap. The Structure from Motion (SfM) technique can utilize overlapping sets of nadir imagery as input. To ensure high-quality results from SfM processing, the typical sidelap and overlap values are set at 75% or greater (Slocum et al., 2019).

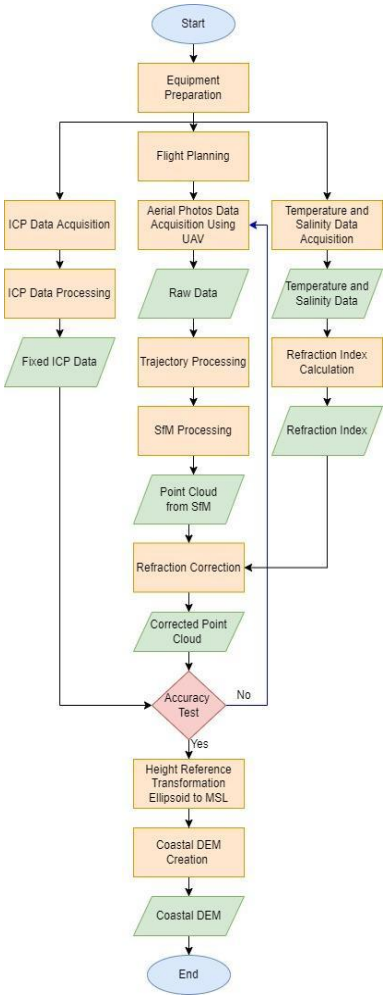

Figure 2 Workflow research

Figure 3 Flight plan at Tidung Island

After creating the flight plans, several control points were plotted to serve as UAV base stations and checkpoints for assessing the accuracy of the generated data.

2.4. Aerial Images Acquisition using the UAV

The UAV system is a multirotor type with four motors and can perform aerial shooting missions autonomously in accordance with the flight plan waypoints that have been made in the planning. The advantage of using a UAV multirotor is that it can take off and land vertically in a very limited area (Syetiawan, 2020).

The UAV used in aerial images on the research area has a range of 20 km by carrying lidar sensors and aerial photogrammetry system. However, in this research, only the results from aerial photogrammetry were used. The aerial images acquisition was carried out with a flying height of 150 meters above ground level and a flight speed of 10 m/s. Takeoff and landing points were selected in areas that are free from obstructions such as trees and other objects that block the visibility (See Figure 4). The aerial images acquisition step was carried out when the sun was not in its nadir position. This time selection was chosen to avoid the reflectance coming from the sunlight reflection on the sea water surface (sunspot) impacting a decent quality of data processing results.

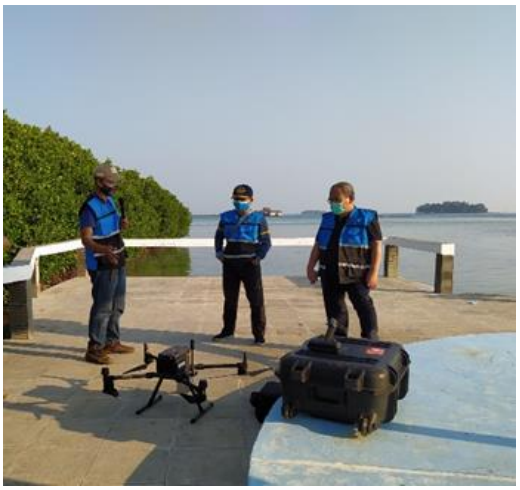

Figure 4 Preparation for aerial images acquisition at Kelapa Island

Before the aerial image acquisition, a base station was established at a known point in the survey area (see Figure 5). The base station is used for post-processing kinematic (PPK) GNSS correction. This setup allows the quality of the trajectory data to be verified immediately after the aerial image acquisition. In this research, Copre software was used to process the trajectory data.

Figure 5 Base station for PPK correction

2.5. Trajectory Processing

The results of the aerial image acquisition include raw aerial image data, GNSS measurement data from the UAV, and results from the Inertial Measurement Unit (IMU). The GNSS data collected on the UAV is processed using the post-processing kinematic method in conjunction with a GNSS base station that has fixed coordinates. The process for determining phase ambiguity employs a combination of forward and backward filtering techniques (Syetiawan, 2020).

Once the GNSS processing yields a fixed solution, the next step involves synchronizing the GNSS time data recorded every second with the GNSS timestamps of the photo exposures. This synchronization ensures the accurate determination of external orientation parameters derived from trajectory data processing using Copre Software. The resulting output consists of exterior orientation parameters.

Additionally, this processing phase involves injecting accurate GNSS position data into the EXIF file of each photo, synchronized with the GNSS data recording results.

2.6. SfM Processing

There are several commercial and non-commercial software that have been developed to process non-metric aerial image data, especially those obtained from the UAV. The software combines two existing methods, namely computer vision algorithms and conventional photogrammetry methods (Papakonstantinou, 2016).

In this research, the authors used Agisoft Photoscan software to process aerial images. This software generates a sparse point cloud (See Figure 6) by identifying distinct structural features in each photo, such as buildings, and matching them across overlapping photos. This method is commonly known as Structure from Motion (SfM).

Figure 6 Sparse point cloud at Pramuka Island

The SfM algorithm automatically determines correspondences between points in overlapping photos using keypoint detection algorithms such as Scale-Invariant Feature Transform (SIFT) (Lowe, 2004) and Speeded-Up Robust Features (SURF) (Bay et al., 2008). By applying the SfM method, the Exterior Orientation parameters are calculated based on these corresponding key points.

Ground Control Points (GCP) are not used in this aerial image processing, so the measured control points will only be used as checkpoints (ICP). So, the source data used is only aerial images data and external orientation resulting from trajectory processing.

After the sparse point cloud is generated, the next step is to generate a dense point cloud with the dense image matching (DIM) method by looking at the suitability of the

pixel hue in each photo that references the previously formed sparse point cloud (See Figure 7).

Figure 7 Dense point cloud at Pramuka Island

2.7. Refractive-Index Value Calculation

The most influential correction factor in estimating bathymetry data from aerial images data is light refraction (Dietrich, 2017). As light passes through the water medium, it bends due to the refractive index of the water. The refractive index of light in seawater is a function of visible light wavelength, temperature, and salinity as described by Equation (1) from McNeil (1977).

$$n(S,T,\lambda) = 1.3247 - 2.5\times 10^{-6}T^2 + S\left(2\times 10^{-4} \times 10^{-7}T\right) + \frac{3300}{\lambda^2} + \frac{3.2\times 10^7}{\lambda^4} \quad (1)$$

where:

n = Refractive index of water
S = Salinity (‰)
T = Temperature (degrees Celsius)
λ = Wavelength of visible light (nm)

In this research, the salinity and seawater temperature parameters were measured using in situ data collection. Sampling was conducted at the deepest depths at each sampling coordinate (see Figure 8). The data were obtained using Valeport SVP Midas equipment (see Figure 9).

Figure 8 Sample distribution of salinity and temperature

Figure 9 Sample acquisition of salinity and temperature

2.8. Refractive Correction

The SfM-processed point cloud data produces a shallower depth than the actual depth. This is due to the refractivity of light by the difference in the medium in seawater. An illustration of the depth of the SfM processing results is illustrated in Figure 10 below.

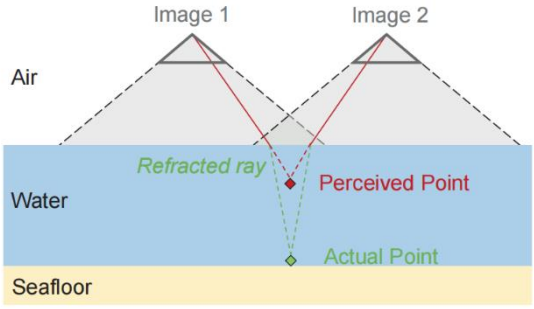

Figure 10 The perceived point cloud Z is shallower than the true location due to uncorrected refractive at the air-water interface (Slocum et al.,2019)

To acquire the actual depth value, the data needs to be refractive-corrected. This correction can be achieved using a trigonometric approach based on the behavior of light as it passes through the air and enters the water. The refractive index for air (n_2) is 1.0, while seawater has a varying refractive index (n_1), which needs to be calculated using Equation (3). An illustration of the process for determining the corrected depth is shown in Figure 11.

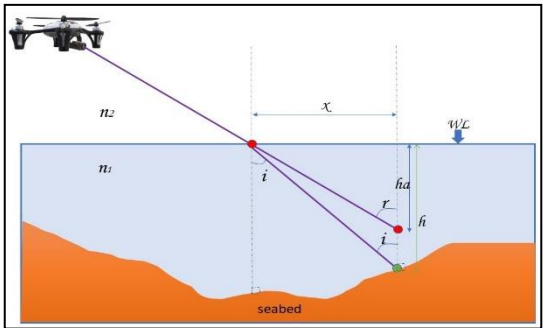

Figure 11 Refractive-corrected depth value determination

Where:

WL = Water level
r = angle of incidence
i = angle of refractive
ha = apparent depth to the SfM point
h = true depth
x = distance from the SfM point to the air/water interface point
n1 = refractive index of seawater
n2 = refractive index of air (1.0)
Zh = depth value with ellipsoid reference

The angle of refractive can be calculated from parameters (See Equation (2)) whose values are known, such as the angle of incidence from the camera orientation direction, refraction index of seawater and refraction index of air (Dietrich ,2017).

$$i = \arcsin(\frac{n2 \sin r}{n1}) \quad (2)$$

Dietrich (2017) illustrates Snell's Law (See Equation (3)) describes the relationship between the angles of incidence and refractive when referring to light or other waves passing through a boundary between two different isotropic media as follows:

$$n1 \sin i = n2 \sin r \quad (3)$$

Woodget et al (2015) proposed a method for refractive correction as much as possible to avoid some of the complications caused using multiple cameras. So, Snell's law is simplified using the small-angle approximation substitution. With a small angle approach, for angles (θ = r || i) less than 10°, sinθ ≅ tanθ as shown in Equation (4) and Equation (5) results in a simplification of Equation (4).

$$\sin i \cong \tan i = \frac{x}{h} \text{ or } \sin r \cong \tan r = \frac{x}{ha} \quad (4)$$

$$h = n1 \times ha \quad (5)$$

Thus, to calculate the elevation of h position referring to the reference system (in this case, ellipsoid height system), it is necessary to reduce the water level. If the water level elevation (WL) used is referenced to the ellipsoid, then the depth value can be calculated by referring to the ellipsoid height (See Equation (6)).

To determine tidal correction using the momentarily water level at the time of acquisition, it can be done by finding the point where the water and land intersect in several locations. Then the elevation value at the intersection point is averaged to get the momentarily sea level elevation value.

The calculation of refractive correction can be performed using software developed by the authors using equation (6), which processes SfM data and is accessible on GitHub by Teguh https://github.com/teguhsulistian/Bathymetric-From-SfM. Moreover, the authors include refraction method by Dietrich from python script (Dietrich, 2016) and the conversation Matlab script (Slocum,2020).

$$Zh = WL - h \quad or \quad Zh = WL - n1xha \quad (6)$$

2.9. ICP Data Acquisition

The ICP data collection uses two methods, namely the RTK GNSS method and the SBES method using the USV vehicle. The RTK GNSS method was used for data acquisition of the topographic and intertidal area data. Although the GNSS measurement using the static method will provide a more precise coordinate value compared to the GNSS measurement using the RTK method, the RTK method can provide coordinate values in real time and quickly (Safi'i, 2018). The ICP on the island is in the form of postmarking on objects, points above the sandy beach, and points of intertidal areas. Some of the ICP collection processes using the RTK method are presented in Figure 12, Figure 13 and Figure 14.

Figure 12 The ICP acquisition at intertidal area

Figure 13 The ICP acquisition at sandy area

Figure 14 The ICP acquisition for postmarking

Meanwhile, the ICP on the shallow waters was acquired using SBES with a USV vehicle because shallow waters are dangerous for conventional survey vessels to sail on. Communication between the vehicle and the control unit on the ground uses telemetry with a factual range of up to 1 km in the field. The sensor used in the sounding is a single beam with a frequency of 200 kHz. The USV positioning using a DGNSS correction signal with an accuracy of 10 cm for the horizontal component.

To mitigate vertical noise, tidal data from temporary tide stations is employed, specifically for the bathymetric survey in the Kepulauan Seribu, conducted by the Center for Mapping of Marine and Coastal Environments under

The Geospatial Information Agency. The process of collecting in situ data using the USV is illustrated in Figures 15 and 16 below.

Figure 15 Deploying process of the USV

Figure 16 USV operating situation

The SBES data processing was carried out using Teledyne PDS software, where noise data was removed to obtain clean data. Once the data was cleaned, tide correction was applied. The SBES data processing workflow is illustrated in Figure 17.

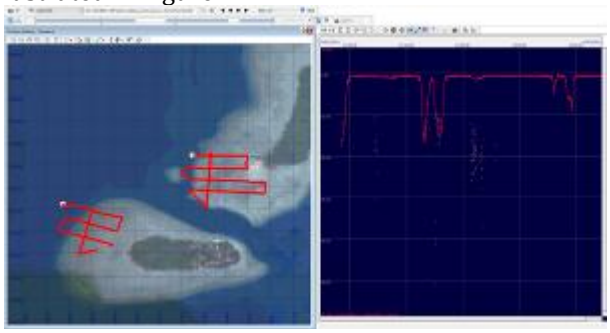

Figure 17 The SBES data processing and distribution of its point

After that, this research will explore the capacity of the UAV compared with sounding by the USV. Then capacity calculation of sounding by the USV is solved using Equation (7) and Equation (8) below.

$$Ks = \frac{As}{Ts} \quad (7)$$

$$Ts = \frac{As \times \frac{1}{Is}}{V} \quad (8)$$

Where:

Ks = Capacity Survey of the USV (km²/hour)
As = Area of survey (km²)
Ts = Duration for survey (hour)
Is = Line interval for the USV mission (km)
V = Speed of the USV (km/hour)

2.10. Accuracy Assessment

The accuracy assessment for both horizontal and vertical components follow the guidelines set by the Regulation of the Geospatial Information Agency (BIG) Number 18 of 2021 on Procedures for Organizing Geospatial Information. The horizontal accuracy of aerial images is evaluated using ICP marked on the islands. Horizontal accuracy is represented by the Circular Error 90% (CE90), which measures horizontal geometric accuracy as the radius of a circle encompassing 90% of the positional errors (see Equation 9). In contrast, vertical accuracy is represented by the Linear Error 90% (LE90), which measures vertical geometric accuracy (height) as the value indicating that 90 % of the height errors fall within this range (see Equation 10).

CE90 and LE90 values can be obtained by the formula referring to the following standards US NMAS (United States National Map Accuracy Standards) as follows:

$$CE90 = 1.5175 \times RMSEr \quad (9)$$

$$LE90 = 1.6499 \times RMSEz \quad (10)$$

where:

RMSEr = Root Mean Square Error in x and y position (horizontal)
RMSEz = Root Mean Square Error in z position (vertical)

The Other accuracy assessment using the estimated confidence level (CI) 95% refers to Equation (11). After that the value of CI 95% compared to Total Vertical Uncertainty (TVU).

$$CI95 = 1.96 \times RMSEz \quad (11)$$

where:

CI95 = The estimate confidence level
RMSEz = Root Mean Square Error in z position (vertical)

The TVU was solved by Equation 12 as specified by the International Hydrographic Organization (IHO) in its Standards for Hydrographic Surveys, S-44 Edition 6.1.0.

$$TVU\ \max = \sqrt{a^2 + (b \times d)^2} \quad (12)$$

where:

TVUmax = maximum allowable TVU
a = represents that portion of the uncertainty that does not vary with the depth
b = a coefficient which represents that portion of the uncertainty that varies with the depth
d = depth

2.11. Generation of Coastal DEM

The generation of the coastal DEM uses a refractive-corrected point cloud and has qualified to the accuracy assessment specifications. This research aims to analyze

whether bathymetry data from aerial images can produce coastal DEM with high resolution. The density of the point cloud is also a consideration in generating a coastal DEM. The generation of DEM using the surface module in GMT is a data-gridding process using adjustable tension continuous curvature splines (Wessel et al., 2019).

3. Result and Discussion

The total coverage of the survey area is 33.346 km^2 including the shallow water areas and land area of the island. Detailed information of survey coverage and total duration of the flight mission is shown on Table 2 below.

Table 2 Survey coverage and duration

Location (island)	Surveyed area (km^2)	Shallow water area (km^2)	Length of flight line (km)	Duration (hour)
Kelapa Dua	1.265	0.864	7.85	0.218
Kelapa and Harapan	6.776	6.334	45.16	1.254
Pramuka	2.962	2.094	17.8	0.494
Panggang	4.630	3.522	2.39	0.066
Tidung Kecil and Besar	14.580	11.934	67.36	1.871
Payung	3.133	2.060	12.72	0.353
Total	**33.346**	**26.808**	**153.28**	**4.257**

Based on Table 2, the capacity of the UAV survey is 7.833 km^2/hour for the total surveyed area and 6.297 km^2/hour specifically for shallow water areas. Moreover, it will be compared if the bathymetric data is acquired using the USV.

The Actual operation speed of the USV is 2.5 knots or equal to 4.63 km/hour (V). Meanwhile, 1 km^2 of the USV survey area needed 40 km survey lines, which assumes if the general survey line interval is 25 m, then the survey line required for 26.808 km^2 of survey area is 1072.32-line km reference to equation (7). So that the time required for the USV is 231.603 hours reference to Equation (8), then it has a capacity of 0.115 km^2/hour. Thus, the survey capacity using the UAV is faster than using the USV. In other words, acquisition using the UAV is more effective and efficient.

UAV trajectory processing for determining fixed position uses post processing kinematic method. The ground base point should be obtained before UAV measurement. Table 3 shows the result of GNSS coordinate for UAV base station.

Table 3 Base Station Coordinate

Benchmark ID	Coordinate	Ellipsoid Height (m)
BM1 (Pulau Kelapa)	5°39'24.28264" S 106°33'54.23509" E	19.953
BM2 (Pulau Pramuka)	5°44'45.45211" S 106°36'43.73310" E	20.246
BM3 (Pulau Tidung)	5°47'58.07849"S 106°29'57.41967"E	19.783

Results from aerial image processing by the SfM method are mosaics of the aerial images and point cloud. The file data format for high-resolution mosaics of aerial images is Geotiff file format (See Figure 18). This file format is supported for advanced analysis in geographic information system (GIS) software. The projection system of the aerial image is UTM Zone 48-South with SRGI2013 datum (Indonesia datum). Pixel resolution of the aerial image is 5 cm x 5 cm with pixel depth 8 bit.

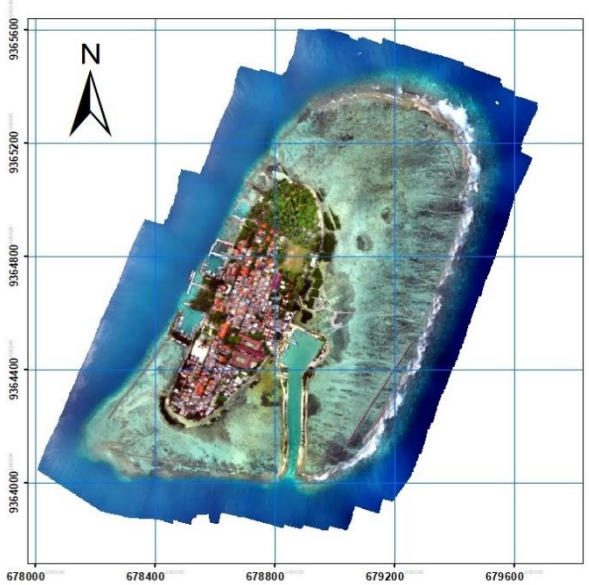

Figure 18 Mosaic of aerial images in Pramuka Island

The point cloud generated from the SfM process has an average point density of 60.576 samples/m^2, with a point spacing of 0.127 m, as shown in Table 3 below. The GSD from aerial image processing is 40 mm (or 4 cm). Given this density and point spacing, the coastal DEM can be generated at a high resolution of 0.5 meters.

Table 3 Density and spacing of point cloud

Location	Density (samples/m^2)	Point Spacing (m)
Kelapa dua Island	56.26	0.133

Location	Density (samples/m²)	Point Spacing (m)
Kelapa dan Harapan Island	59.84	0.122
Pramuka Island	63.83	0.125
Panggang Island	54.71	0.135
Tidung Kecil dan Besar Island	61.24	0.127
Payung Island	67.58	0.121
Average	**60.576**	**0.127**

Point cloud results contain coordinates (X, Y, Z), object classification, and color information (RGB), all of which are stored in LAS file format. As shown in Figure 19, the topographic and shallow bathymetry data are consistent and well-integrated. However, in deeper water areas, the point cloud exhibits noise, as the SfM method is unable to process data in these regions effectively. Additionally, noise cleaning and filtering of objects on the water (such as boats, cages, navigation aids, etc.) must be performed, as these can interfere with the refractive correction processing.

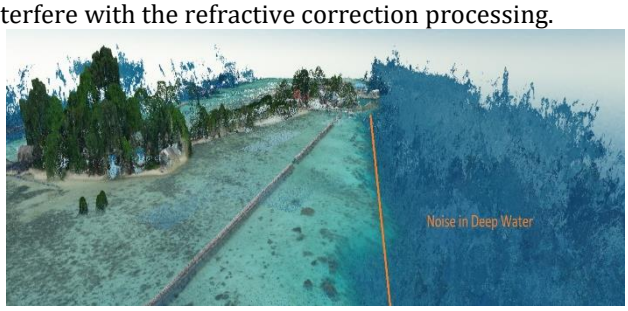

Figure 19 Point cloud from SfM process

The next step is refractive correction to determine the true depth. The depth from point cloud SfM still assumes in apparent depth refer to figure above. Salinity and temperature samples were collected from several points within the research area. The salinity and temperature values should be measured up to a depth of 15 meters below the water surface. For this research, the wavelength of visible light used is 589.3 nanometers. The average salinity value recorded was 32.748 ‰, while the average temperature was 30.170 °C from table 4. Using these parameters, the refractive index of seawater (n1) was calculated to be 1.33742085, as determined by Equation (3).

Table 4 Temperature and Salinity Result

Depth (m)	Sound Velocity (m/sec)	Temperature (C)	Salinity (‰)
0.027	1543.784	30.016	33.192
0.169	1543.769	30.157	32.891
0.165	1543.758	30.216	32.763
0.184	1543.756	30.243	32.707
0.226	1543.76	30.258	32.68
0.246	1543.732	30.266	32.637
0.236	1543.761	30.265	32.667
0.472	1543.793	30.267	32.69
0.529	1543.768	30.269	32.661
0.612	1543.78	30.27	32.669
0.687	1543.793	30.278	32.662
0.663	1543.778	30.284	32.636
0.669	1543.774	30.278	32.644
0.68	1543.768	30.275	32.644
0.677	1543.766	30.273	32.646
0.664	1543.766	30.272	32.651
0.663	1543.768	30.273	32.651
0.728	1543.779	30.282	32.64
0.688	1543.775	30.279	32.643
0.676	1543.79	30.278	32.66
0.719	1543.799	30.287	32.65
0.645	1543.767	30.281	32.632
0.684	1543.798	30.274	32.675
0.739	1543.814	30.28	32.678
0.674	1543.807	30.28	32.672
0.64	1543.792	30.279	32.66
0.747	1543.831	30.289	32.676
0.765	1543.827	30.294	32.662
0.681	1543.793	30.295	32.629
0.72	1543.817	30.291	32.659
0.828	1543.829	30.306	32.639
0.721	1543.799	30.305	32.614
0.697	1543.804	30.295	32.639
0.853	1543.825	30.29	32.667
0.771	1543.803	30.297	32.633
0.693	1543.777	30.292	32.619
0.81	1543.833	30.286	32.683
0.81	1543.814	30.296	32.645
0.751	1543.824	30.303	32.642
0.761	1543.834	30.297	32.663
0.837	1543.825	30.3	32.647
0.838	1543.837	30.304	32.651
1.191	1543.804	30.308	32.605
1.929	1543.498	30.221	32.472
2.697	1543.473	30.09	32.697

Depth (m)	Sound Velocity (m/sec)	Temperature (C)	Salinity (‰)
3.742	1543.61	30.046	32.901
4.329	1543.559	30.003	32.93
5.331	1543.469	29.96	32.913
6.205	1543.342	29.892	32.913
7.095	1543.324	29.84	32.986
8.473	1543.342	29.809	33.043
9.224	1543.322	29.787	33.058
10.674	1543.294	29.765	33.052
11.899	1543.323	29.757	33.076
13.029	1543.32	29.747	33.075
13.537	1543.324	29.736	33.092
14.209	1543.342	29.736	33.099
15.519	1543.357	29.733	33.098
Average	**1543.689**	**30.170**	**32.748**

Refractive correction in SfM point cloud solved by Equation (6) using refractive index from in situ data. The water level is determined based on acquisition aerial image time. The vertical reference while correction applied is ellipsoid height vertical reference. The refractive correction was processed using SfM Bathymetry software by the authors (available on Github). A comparison between the point clouds before and after applying the refractive correction is shown in Figure 21 below.

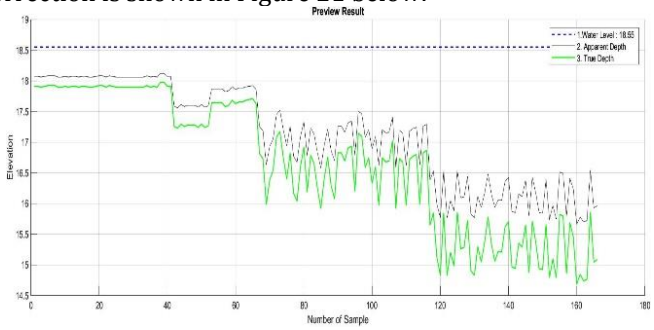

Figure 21 Comparing uncorrected and corrected data

Based on the Figure 21 above, the elevation value from corrected data is deeper than uncorrected data. These results show us that Snell's law can be applied for point cloud data from SfM refractive correction. However, for further analysis, the deviation between corrected and uncorrected data is linear with increasing depth as shown in the linear regression graph below (See Figure 22).

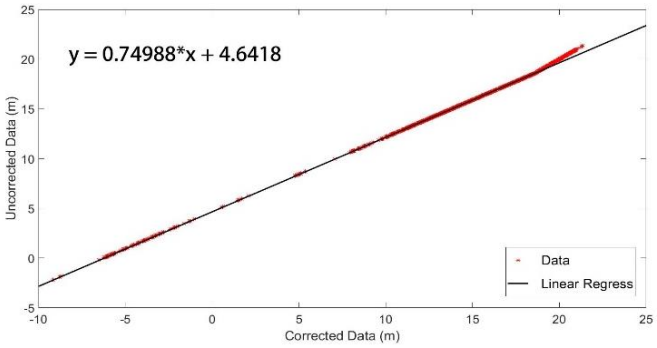

Figure 22 Linear regression graph between corrected and uncorrected data

Accuracy assessment for corrected point cloud using ICP to determine the level of data accuracy. The horizontal component was evaluated using postmarked ICP data visible in the aerial images. The result of horizontal accuracy assessment can be seen in the Table 5.

Table 5 The result of horizontal accuracy

Number Of Sample (Points)	28
RMSEr (m)	0.103
Accuracy CE90%	0.156

Meanwhile, for vertical accuracy assessment using ICP from RTK GNSS measurement intertidal area and sounding using the USV in shallow water areas. The vertical accuracy result can be seen in Table 6 below.

Table 6 The result of vertical accuracy

Number Of Samples (Points)	7228
RMSEz (m)	0.191
Accuracy LE90% (m)	0.315

Furthermore, the consistency between corrected point data and sounding data can be seen in Figure 23. Furthermore, R^2 value is the coefficient of determination, which is a statistical measure that indicates how well a regression model explains the variation in a dependent variable. The R^2 value of SfM point cloud data compared to sounding data is 0.86567, which is a number close to 1 indicating a perfect fit between the model and the data.

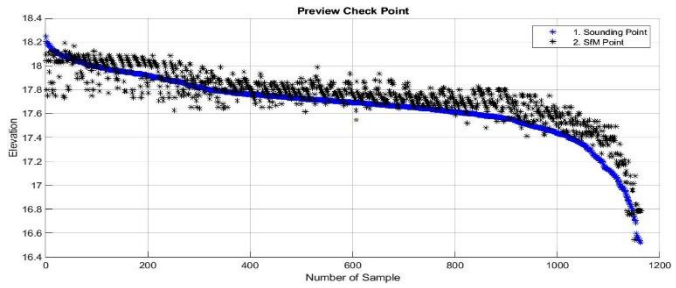

Figure 23 Consistency between corrected point and sounding data

Thereafter, for TVU of bathymetry data from SfM method compared to sounding data can be seen on the Table 6 below. Average depth is determined 0-5 meters refer to consistency between corrected data and sounding data (See Figure 23). The estimated confidence interval (CI) 95% based on Equation 12 is 0.375.

Table 6 The Result of TVU

Component	Order-2	Order-1	Order-1a	Special Order	Exclusive Order
a	1	0.5	0.5	0.25	0.15
b	0.023	0.013	0.013	0.0075	0.0075
TVUmax	1.01	0.50	0.50	0.25	0.15
Compile	YES	YES	YES	NO	NO

Refer to Table 6 above, the bathymetry data from SfM can be classified into IHO order-2, order-1 and order-1a. Attention must be paid to point density and point spacing to ensure the ability to detect objects according to Order-1a, which requires a resolution of less than 2 meters. Additionally, the coastal DEM is designed to achieve a resolution of 0.5 meters.

The coastal DEM has been generated using spline interpolation method with a tension parameter 0.36 (See Figure 25). Before generating coastal DEM, the point cloud SfM data must be transformed to the vertical reference of Mean Sea Level (MSL). The correction value between ellipsoid and MSL is 18.887 meters (see figure 24).

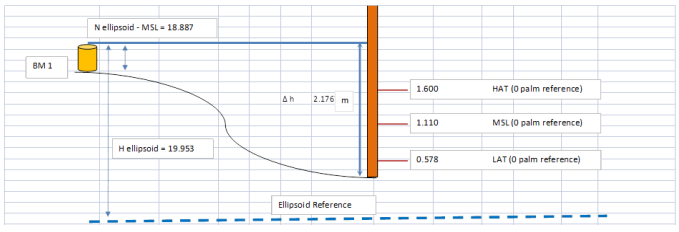

Figure 24 Tide datum and ellipsoid relationship diagram

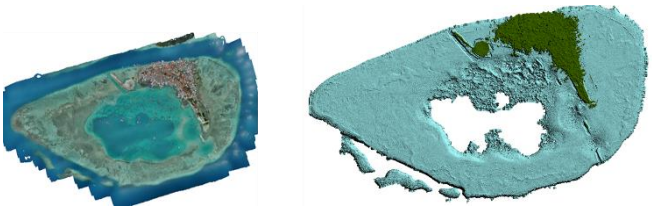

Figure 25 Coastal DEM

4. Conclusion

The conclusions of this research are categorized into three main aspects: data acquisition capacity, data resolution level, and data accuracy level.

In terms of data acquisition capacity, the use of a UAV for data collection in shallow water areas proves to be significantly faster than utilizing a USV. Additionally, the UAV proves to be more effective and efficient in terms of both cost and time. The UAV has a data acquisition capacity of 6.297 km^2/hour, compared to the USV's capacity of 0.115 km^2/hour.

Regarding the data resolution level, the bathymetry data obtained using the SfM method demonstrates a high level of resolution in terms of point density, point spacing, and Ground Sampling Distance (GSD). The point density is 60.576 samples/m^2, the point spacing is 0.127 meters, and the GSD is 4 cm. Based on this point density and spacing, a coastal DEM with a resolution of 0.5 meters can be generated.

Finally, concerning the accuracy level, the accuracy of the SfM bathymetry data shows consistency when compared with USV sounding data up to a depth of 5 meters. The resulting data meets the requirements for basemaps at a scale of 1:5000. Furthermore, the SfM bathymetry data complies with the International Hydrographic Organization (IHO) S-44 standards for Order-2, Order-1, and Order-1a surveys.

However, there are certain limitations to using the SfM method for bathymetry data extraction. It is most effective in areas with clear water, low waves, minimal surface obstructions, and specific timing to avoid sunspots during data acquisition.

5. Competing Interests

The authors declare no competing interest in this article.

6. Reference

Awadallah, M.O.M. (2021). *Comparison between the Green and the Red LiDAR terrain models in flood inundation estimations*. Master's thesis of Mahmoud Omer Mahmoud Awadallah at Norwegian University of Science and Technology, Department of Civil and Environmental Engineering.

Bay, H., A. Ess, T. Tuytelaars, and L. Van Gool. (2008). *Speeded-up robust features (SURF)*. Computer Vision and Image Understanding 110(3):346–359.doi: 10.1016/j.cviu.2007.09.014.

Dietrich, J.T. (2016). py_sfm_depth homepage. http://github.com/geojames/py_sfm_depth.

Dietrich, J.T. (2017). *Bathymetric structure-from-motion: extracting shallow stream bathymetry from multi-view stereo photogrammetry*. Earth Surface Processes and Landforms 42(2):355–364. doi:10.1002/esp.4060.

Gularso, H., Parapat, A.D., Sulistian, T., Atmaja, A.A. (2021). *Penentuan Garis Pantai Menggunakan Foto Udara Dari Wahana Tanpa Awak: Studi Kasus Pantai Ujong Batee Aceh* [Determination of Shoreline Using Unmanned Aerial Vehicle: Case Study Ujong Batee Aceh Beach]. National Seminar of Geomatica 2021. DOI: 10.24895/SNG.2020.0-0.1185.

International Hydrographic Organization. (2022). *Standards for Hydrographic Surveys* (S-44 Edition 6.1.0). Retrieved from https://iho.int/uploads/user/pubs/standards/s-44/S-44_Edition_6.1.0.pdf

Lingua, A.M., Maschio, P., Spadaro, A., Vezza, P., Negro, G. (2023). *Iterative Refraction-Correction Method On Mvs-Sfm for Shallow Stream Bathymetry*. The International Archives of the Photogrammetry, Remote Sensing and Spatial Information Sciences, Volume XLVIII-1/W1-2023 12th International Symposium on Mobile Mapping Technology (MMT 2023), 24–26 May 2023, Padua, Italy.

Lowe, D.G. (2004). *Distinctive Image Features from Scale Invariant Keypoints*. International Journal of Computer Vision 60(2):91–110. doi:10.1023/B:VISI.0000029664.99615.94.

Matsuba, Y., and S. Sato. (2018). *Nearshore bathymetry estimation using UAV*. Coastal Engineering Journal 60(1):51–59. doi:10.1080/21664250.2018.1436239.

McNeil ., G.T. (1977). *Metrical fundamentals of underwater lens system*. Opt. Eng. 16, 128–139 119772.

Nugraha, W., Parapat, A.D., Arum, D.S., & Istighfarini, F. (2018). *GNSS RTK application to determine coastline case study at Northern Area of Sulawesi and Gorontalo*. E3S Web Conf., 94 (01016), 1-7. International Symposium on Global Navigation Satellite System 2018 (ISGNSS 2018). Bali. https://doi.org/10.1051/e3sconf/20199401016.

Papakonstantinou, A., K. Topouzelis, and G. Pavlogeorgatos. (2016). *Coastline Zones Identification and 3D Coastal Mapping Using UAV Spatial Data*. International Journal of Geo-Information.

Pratiwi, D.M. (2016). *Analisis Hasil Pengukuran Posisi Horizontal Kapal USV "Arossel" (Autonomous Remotely Operated Surface Vessel) Mengacu Standar IHO Untuk Pemetaan Batimetri Skala Besar* [Analysis of Horizontal Position Measurement Results on USV "Arossel" (Autonomous Remotely Operated Surface Vessel) refer to IHO standard for Large Bathymetry Mapping]. Undergraduate thesis Gadjah Mada University. Yogyakarta.

Safi'i, A.N. (2018). *Akurasi Pengukuran GPS Metode RTK-NTRIP Menggunakan CORS BIG* [Accuracy of GPS Measurement RTK-NTRIP Method Using BIG CORS]. National Seminar of Geomatica 2018. DOI: 10.24895/SNG.2017.2-0.441.

Slocum, R.K. (2020). *Source Code at* https://github.com/hokiespurs/sfmrefract.git.

Slocum, R.K., W. Wright, C. Parrish, B. Costa, M. Sharr, and T.A. Battista. (2019). *Guidelines for Bathymetric Mapping and Orthoimage Generation using sUAS and SfM, An Approach for Conducting Nearshore Coastal Mapping*. NOAA Technical Memorandum NOS NCCOS 265. Silver Spring, MD. 83 pp. doi:10.25923/07mx-1f93.

Storlazzi, C.D., Dartnell, P., Hatcher, G.A., Gibbs, A.E. (2016). *End of the chain? Rugosity and fine-scale bathymetry from existing underwater digital imagery using structure-from-motion (SfM) technology*. Coral Reefs (2016) 35:889–894.https://doi.org/10.1007/s00338-016-1462-8

Syetiawan, A., H. Gularso, G. I. Kusnadi and G. N. Pramudita. (2020). *Precise Topographic Mapping Using Direct Georeferencing in UAV*. The Fifth International Conferences of Indonesia Society for Remote Sensing.

Terama, E., Peltomaa, J., Mattinen-Yuryev, M and Nissinen, A. (2019). Urban Sustainability and the SDGs: A Nordic Perspective and Opportunity for Integration. Urban Sci. 2019, 3, 69; doi:10.3390/urbansci3030069.

Wessel, P., Luis, J.F., Uieda, L., Scharroo, R., Wobbe, F., Smith, W.H.F., & Tian, D. (2019). *The generic mapping tools version 6*. Geochemistry, Geophysics, Geosystems, 20(11), 5556-5564. https://doi.org/10.1029/2019GC008515.

Woodget AS, Carbonneau PE, Visser F, Maddock IP. 2015. *Quantifying submerged fluvial topography using hyperspatial resolution UAS imagery and structure from motion photogrammetry*. Earth Surface Processes and Landforms 40: 47–64. DOI:10.1002/esp.36.